Uncertainty Quantification of Input Parameters in a 2-D Finite-Element Model for Broken Rotor Bar in an Induction Machine

Md Masum Billah[1], Floran Martin[1], Anouar Belahcen[1,2], Aswin Balasubramanian[1], Toomas Vaimann[2], and Jan Sobra[3]

[1]Department of Electrical Engineering and Automation, Aalto University, 02150 Espoo, Finland
[2]Department of Electrical Power Engineering and Mechatronics, Tallinn University of Technology, 19086 Tallinn, Estonia
[3]Department of Power Electronics and Machines, University of West Bohemia, 30100 Plzen, Czech Republic

In this article, a forward uncertainty propagation method is presented for a 2-D finite-element (FE) model in an induction machine. This method is applied to quantify the uncertainty of input parameters, for example, dimensions and material properties, and demonstrate their variability effect on harmonics related to the broken rotor bar (BRB) faults. To show the most influential input parameters in the case of BRB harmonics, a global sensitivity analysis is performed from the polynomial chaos expansion (PCE) approximation of the FE model. The results of this study indicate that BRB harmonics are highly sensitive to stator inner diameter, rotor outer diameter, rotor bar conductivity, and core materials. Moreover, the combined variability of these sensitive input parameters can attenuate the amplitude of the BRB harmonics 30%–90% compared to the simulation results at nominal values of input parameters and closely match with measurement results.

***Index Terms*— Broken rotor bar (BRB), finite-element (FE) model, forward uncertainty propagation, polynomial chaos expansion (PCE), sobol sensitivity analysis.**

I. Introduction

BROKEN rotor bar (BRB) faults in an induction machine can be critical due to their degenerative nature if the diagnosis procedure cannot be performed in the incipient stage. The diagnosis of BRB faults has been mostly performed in the induction machine through motor current signature analysis (MCSA) [1]. Recently, data-driven machine learning (ML) methods are becoming more popular due to fully automatic faults analysis and better prediction accuracy even in harsh operating conditions [2]. However, the key problem of ML methods is that they require a substantial amount of data in the training phase.

Realistic BRB faults data can be extracted by constructing a measurement platform where faults are typically implemented artificially. However, constructing such a measurement setup is a laborious and expensive process. A deterministic simulation model, for example, the 2-D finite-element (FE) model of BRB can be a viable solution to produce a large amount of labeled synthetic data for any arbitrary operating conditions. Nevertheless, significant deviation may exist between features, for example, the amplitude and frequency of the harmonics of simulated and measured BRB faults data, which are often treated as important features in ML methods [2], [3]. Such deviation may lead to poor performance of ML methods in the diagnosis of BRB faults. The frequency and amplitude deviation of BRB harmonics may arise in the 2-D FE model due to model discrepancies such as neglecting the effect of speed ripple phenomenon, skewness of the rotor bar, and inter bar current [4]. In addition, the magnetic saturation level tends to lower the effect of BRB harmonics [5].

Furthermore, uncertainty may exist in input parameters such as machine dimensions and material properties due to manufacturing defects, stresses, or aging during their operational lifetime [6]–[8]. As a result, the nominal values of these parameters may deviate and lead to inaccurate estimation of the amplitude of BRB harmonics. The model discrepancies in the 2-D FE model of BRB and the effect of magnetic saturation level on BRB harmonics were well studied in [4] and [5]; however, no attempt has been made to investigate the amplitude variability of BRB harmonics comprehensively due to the uncertainty of input parameters.

We addressed the variability problem of input parameters in the 2-D FE model of BRB and analyzed their impact on BRB harmonics comprehensively. The proposed non-intrusive approach provides great flexibility to calibrate the input parameters without modifying the FE model. The major contribution of this article comes from: 1) analyzing the existing deviation between FE simulated and measured BRB faults data through the MCSA method; 2) identifying sensitive input parameters to the BRB harmonics by performing Sobol sensitivity analysis from the polynomial chaos expansion (PCE) approximation of the high-dimensional FE model; and 3) quantifying uncertainty and calibrating the obtained sensitive input parameters to minimize the deviation in between simulated and measured BRB data.

II. Methodology

A. Measurements

The measurement setup was accomplished with two induction machines having the same rating as the simulated one. One induction machine was acting as a motor where BRB

Manuscript received 2 February 2022; revised 24 March 2022; accepted 2 May 2022. Date of publication 9 May 2022; date of current version 26 August 2022. Corresponding author: M. M. Billah (e-mail: md.billah@aalto.fi).

Color versions of one or more figures in this article are available at https://doi.org/10.1109/TMAG.2022.3173663.

Digital Object Identifier 10.1109/TMAG.2022.3173663

This work is licensed under a Creative Commons Attribution 4.0 License. For more information, see https://creativecommons.org/licenses/by/4.0/

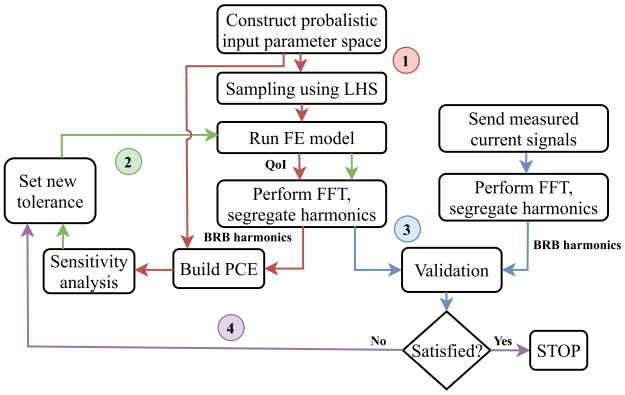

Fig. 1. Flowchart of the proposed uncertainty propagation scheme.

faults were implemented, and another machine was working as a load. The tested machine was fed from the grid supply, and the loading machine was connected through an industrial drive for the flexibility of the load variations. Details of the measurement setup are provided in [1]. In this article, the grid-fed data for one and two BRB faults at full load conditions are utilized for validation purposes.

B. Proposed Uncertainty Propagation Scheme

The flowchart of the proposed forward uncertainty propagation method for the 2-D FE model of BRB is shown in Fig. 1. In step 1, a probabilistic input space is constructed for each input parameter through a uniform probability distribution function (pdf). Random realizations are drawn from the probabilistic input spaces using the Latin Hypercube Sampling (LHS) method. The advantage of the LHS method is that it requires fewer samples to sufficiently explore the input probabilistic space, which significantly reduces the computational cost. Thanks to the randomization method, the 2-D deterministic FE model can be employed for analyzing the uncertainty propagation.

The quantity of interest (QoI) is the random time-domain stator current signals, which are transformed into the frequency domain by performing the fast Fourier transformation (FFT). Then, BRB harmonic components are segregated from other harmonic components present in the frequency-domain signals. Afterward, the random amplitude of BRB harmonic components are served as the output to build the PCE surrogate model. The Sobol sensitivity analysis indices are computed to identify the most sensitive parameters to the BRB harmonics from the PCE surrogate model. In step 2, a new tolerance level is set to only sensitive input parameters and propagated through the FE model deterministically. Subsequently, the FFT of QoI is performed, and BRB harmonics are segregated to validate the simulated and measured results in step 3. In step 4, the calibration process is continued with steps 2 and 3, respectively, until the amplitude of simulated BRB harmonics is closely matched with the measurement results.

The list of selected input parameters for the calibration is provided in Table I. Uniform distribution $U(\theta_{\min}, \theta_{\max})$ is formed between the lower $\theta_{\min}$ and upper $\theta_{\max}$ bounds for each input parameter according to the initial tolerance level as mentioned in Table I. The probabilistic uncertainty model of the B-H (i.e., B is the magnetic flux density, and H is the magnetic field strength) curve is realized by scaling the flux density values of a reference material law by $\boldsymbol{B}_i = (1 + \delta_i)\boldsymbol{B}_{\text{ref}}$, where $\boldsymbol{B}_{\text{ref}}$ represents the flux density values $B_0, \ldots, B_{23}$ in the B-H curve mentioned in Table I, and $i = 1, 2, 3, \ldots, 200$ is the number of realizations [8]. The stochastic variable δ_i is drawn from a uniform distribution in the range $\pm 15\%$ with the LHS method. Since the reference material law is strictly monotonous, the 200 random scaled realizations preserve this property. The 24 flux density values are plugged into the input parameters $\theta_{23}, \ldots, \theta_{46}$. The knee of the B-H characteristic is found in parameters $\theta_{25}, \ldots, \theta_{28}$. The variability is introduced only in the magnetic flux density $\boldsymbol{B}$ and the magnetic field strength $\boldsymbol{H}$ remains constant, which also assists to preserve the monotonicity for individual generated B-H curve.

TABLE I
LIST OF INPUT PARAMETERS FOR CALIBRATION

Parameter	Symbol	Nominal value	Tolerance
Stator slot:			
Opening height	θ_1	0.7 mm	$\pm 10\%$
Opening width level 1	θ_2	2.8 mm	$\pm 2\%$
Opening width level 2	θ_3	4 mm	$\pm 3\%$
Depth	θ_4	24 mm	$\pm 1\%$
Opening width level 3	θ_{20}	6.8 mm	$\pm 2\%$
Height	θ_{21}	28.3 mm	$\pm 2\%$
Rotor slot:			
Depth	θ_6	12 mm	$\pm 1\%$
Opening height	θ_7	0.2 mm	$\pm 10\%$
Opening width level 1	θ_8	1 mm	$\pm 4\%$
Opening width level 2	θ_9	4.4 mm	$\pm 1\%$
Opening width level 3	θ_{10}	2 mm	$\pm 2\%$
End-ring:			
Cross-sectional area	θ_{11}	375 μm^2	$\pm 5\%$
Radial height	θ_{12}	25 mm	$\pm 5\%$
Average diameter	θ_{13}	98 mm	$\pm 5\%$
Stator inner diameter	θ_5	125 mm	$\pm 5\%$
Rotor outer diameter	θ_{22}	123.6 mm	$\pm 5\%$
Sheet fill factor	θ_{14}	0.98	$\pm 5\%$
Average length of a coil	θ_{18}	415 mm	$\pm 5\%$
Rotor inertia	θ_{19}	0.4 kg.m^2	$\pm 10\%$
Rotor bar conductivity	θ_{15}	25.8 MS/m	$\pm 10\%$
Stator resistance	θ_{16}	0.15 Ω	$\pm 10\%$
End-winding reactance	θ_{17}	0.0417 Ω	$\pm 10\%$
***B-H* curve:**			
B_0, B_1	θ_{23}, θ_{24}	0.0, 0.5 T	$\pm 15\%$
$B_2, ..., B_5$	$\theta_{25}, ..., \theta_{28}$	0.9:0.1:1.2 T	$\pm 15\%$
$B_6, ..., B_{23}$	$\theta_{29}, ..., \theta_{46}$	1.25:0.05:2.1 T	$\pm 15\%$

A four-pole, 50 Hz, 333 V, 18 kW induction machine with the skewed rotor bars is simulated by an in-house 2-D FE simulation software *fcsmek*. To simulate BRB faults, a three-phase sinusoidal voltage supply is applied to the machine terminal, and the three-phase stator current is computed as an unknown quantity through the time-stepping method. The BRB faults are implemented by setting the resistance of the specific bars to a very high value in the circuit equation of the rotor cage. This results in zero net current; however, the eddy current still presents in the BRBs. Due to BRBs, the anomalous current starts to flow through the neighboring bars, which causes unbalanced magnetic field distribution in the rotor core. Details of BRB faults modeling in the 2-D FE model are provided in [9]. Stochasticity is introduced by extracting 200 realizations from each probabilistic input space and propagating through the 2-D FE model of BRB. Each simulation is performed for 16.14 s with a sampling frequency

of 10 kHz. The resulted random time-domain current signals are transformed into frequency-domain by using FFT.

The harmonics present in the stator current are segregated roughly into three categories such as supply harmonics, slot harmonics, and BRB harmonics. The harmonics which are multiples of the supply frequency f_s stated as supply harmonics f_{sh} such that $f_{\text{sh}} = kf_s$, where $k = 1, 2, 3, \ldots$ is the harmonic indices. The high-frequency principal slot harmonics f_{psh} are produced due to the slotting effect of the machine and can be expressed as $f_{\text{psh}} = f_s(kN_r((1-s)/p) + n_w)$, where N_r is the number of rotor slots, p is the number of pole pairs, s is the slip, and $n_w = \pm 1, \pm 3, \ldots$ is the order of stator winding distribution harmonics. The fault harmonics due to BRB appears in the stator current signal depending on slip s and supply frequency f_s such that $f_{\text{BRB}} = f_s(1 \pm 2ks)$.

The randomness of true simulation model output $\boldsymbol{y}^{\boldsymbol{M}}(\boldsymbol{\theta})$ can be approximated by a finite series of polynomial expansion

$$\boldsymbol{y}^{\boldsymbol{M}}(\boldsymbol{\theta}) \approx \hat{\boldsymbol{y}}(\boldsymbol{\theta}) = \sum_{i=1}^{P} \alpha_i \Psi_i(\boldsymbol{\theta}) \tag{1}$$

where $\boldsymbol{\theta} = [\theta_1, \theta_2, \ldots, \theta_n]$ are n-D random input variables, $\boldsymbol{y}^{\boldsymbol{M}}(\boldsymbol{\theta})$ are the random output variables (BRB harmonics), P is the truncated polynomial order, $\boldsymbol{\Psi}$ is the known orthogonal polynomial basis function, and $\hat{\boldsymbol{\alpha}}$ represents unknown coefficients. Thanks to their orthogonal properties, the Legendre polynomial basis is suitable one for the uniform pdf, which allows efficient computation and faster convergence rate for error minimization [10]. The unknown coefficients $\hat{\boldsymbol{\alpha}}$ can be estimated deterministically through the regression analysis with the cost function

$$\hat{\boldsymbol{\alpha}} = \arg\left(\min \mathbb{E}\left[\left(\boldsymbol{y}^{\boldsymbol{M}}(\boldsymbol{\theta}) - \hat{\boldsymbol{y}}(\boldsymbol{\theta})\right)^2\right]\right) \tag{2}$$

where $\mathbb{E}[\cdot]$ is the expectation. The orthogonal matching pursuit (OMP) regression method is used to determine the unknown coefficients $\hat{\boldsymbol{\alpha}}$ [11]. However, other methods such as least angle regression (LARS) can also be used to obtain the PCE coefficients $\hat{\boldsymbol{\alpha}}$ [12]. The PCE surrogate model is constructed for individual random BRB harmonics separately, so that the sensitivity analysis indices can be estimated independently. The accuracy and prediction quality of the constructed PCE metamodel for the truncated polynomial order $P = 5$ is ensured by obtaining the validation error using leave-one-out-cross-validation (LOOCV) [12].

According to [13] and [14], the PCE model output $\hat{\boldsymbol{y}}(\boldsymbol{\theta})$ associated with random input parameters $\boldsymbol{\theta} = [\theta_1, \theta_2, \ldots, \theta_n]$ can be decomposed into summands of higher-order dimensions by

$$\hat{\boldsymbol{y}}(\boldsymbol{\theta}) = y_o + \sum_{i=1}^{n} y_i(\theta_i) + \sum_{1 \le i \le j \le n} y_{ij}(\theta_i, \theta_j) + \cdots + y_{1,2,\ldots,n}(\theta_1, \ldots, \theta_n). \tag{3}$$

The first-order and total order Sobol indices can be computed from the total variance of model output in (3) and the conditioned variances as follows:

$$S_i = \frac{\text{Var}[\mathbb{E}[y|\theta_i]]}{\text{Var}[y]}, \quad S_{T_i} = \frac{\text{Var}[\mathbb{E}[y|\boldsymbol{\theta}_{\sim i}]]}{\text{Var}[y]} \tag{4}$$

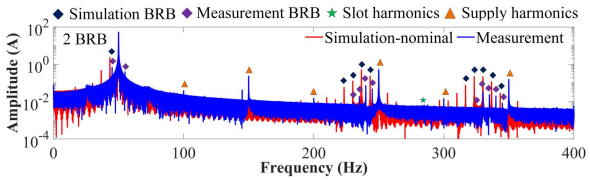

Fig. 2. Segregation of harmonics in the stator current signal is indicated by different markers. Two BRB data from 2-D FE simulation (using nominal values of the input parameters) and measurement at full load are used for the harmonics segregation. Note the logarithmic scale for the y-axis.

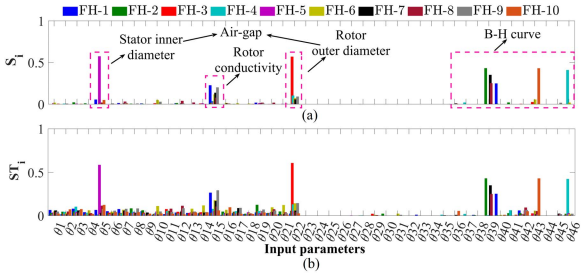

Fig. 3. Sobol sensitivity analysis of ten BRB harmonics that appear in the frequency spectrum range 0–400 Hz of the stator current signal. (a) First-order S_i indices. (b) Total order ST_i indices. Higher index value indicates the most influential input parameters.

where $\boldsymbol{\theta}_{\sim i} = \boldsymbol{\theta} \backslash \theta_i$ means the sensitivity measures for all other variables except the variable θ_i, and $\text{Var}[\cdot]$ is the total output variance, and $\text{Var}[\cdot|\cdot]$ and $\mathbb{E}[\cdot|\cdot]$ represent the conditional variance and expectation, respectively. The first term S_i indicates the main effect of each input parameter θ_i alone, and the latter term S_{T_i} introduces the additional effect of individual input parameters considering the possible interactions with other parameters $\boldsymbol{\theta}_{\sim i}$ alongside their main effect. The higher value of indices S_i and S_{T_i} indicates that the parameters are more influential to the output. If the indices are purely additive (i.e., no interaction among input parameters), then $S_i = S_{T_i}$, and the sum of the first-order indices are $\sum_{i=1}^{n} S_i = 1$, otherwise $\sum_{i=1}^{n} S_i < 1$. In the case of PCE, the Sobol indices in (4) can be estimated straightforwardly from the expansion coefficients $\boldsymbol{\alpha}$ in the post-processing stage [6], [14]. To obtain the Sobol sensitivity analysis indices, we incorporated the sensitivity analysis toolbox from UQL_{AB} [15].

III. Application and Validation

BRB faults and other harmonics are segregated and presented in Fig. 2. Besides the BRB harmonics, supply harmonics have appeared in both simulated and measured signals. Moreover, slot harmonics are produced in the simulation due to neglecting the skewness of the rotor bar. Fig. 2 shows that the BRB harmonics deviate between simulated and measured data in terms of amplitude and frequency.

Fig. 3(a) and (b) shows the first-order and total order Sobol indices for two BRB data at full load. It should be noted that the first-order and total order Sobol indices are computed for individual random BRB harmonics separately. The obtained results are presented together for the first ten BRB harmonics in Fig. 3. It can be seen that few input parameters namely stator inner diameter θ_5, rotor outer diameter θ_{22}, rotor bar conductivity θ_{15}, and B-H curve data θ_{39}, θ_{40}, θ_{43}, and θ_{46} from saturation region have significant impact on the amplitude

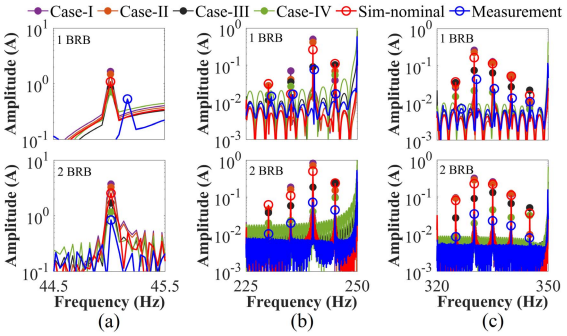

Fig. 4. Calibration of the amplitude and frequency deviation of one and two BRB harmonics at full load. Only BRB harmonics appear in the frequency spectrum range 0–400 Hz of the stator current signal are presented. (a) First BRB harmonic. (b) Second to fifth BRB harmonics. (c) Sixth to tenth BRB harmonics.

TABLE II
INVESTIGATED CALIBRATION CASES IN THE 2-D FE MODEL OF BRB

Parameter	Case-I	Case-II	Case-III	Case-IV
Air-gap $(\theta_5 - \theta_{22})$	7.5%	5%	-5%	-7.5%
Rotor bar conductivity (θ_{15})	25%	15%	-15%	-25%
B-H curve $(\theta_{23}, ..., \theta_{46})$	25%	15%	-15%	-25%

of BRB harmonics. Due to high interaction among these input parameters, first-order Sobol indices are not purely additive; hence, the sum of first-order Sobol indices for each harmonic is $\sum_{i=1}^{n} S_i < 1$. Total order Sobol indices serve the additional impact of each input parameter alongside their main effect which are caused due to their interaction with other parameters. Nevertheless, the main influence of the obtained sensitive input parameters remains the same.

To investigate the variability impact, we studied four calibration cases where the nominal values of the air gap (θ_5–θ_{22}), rotor bar conductivity θ_{15}, and the B-H curve $(\theta_{23}, \ldots, \theta_{46})$ are varied with a certain degree of uncertainty as reported in Table II. The air gap is introduced as a function of stator inner diameter and rotor outer diameter to avoid overlapping between these two parameters. In addition, B-H curve data $(\theta_{23}, \ldots, \theta_{46})$ are varied with respective tolerance levels to avoid monotonicity issues. The obtained results of one and two consecutive BRB faults for four calibration cases are presented in Fig. 4 and compared with simulation (nominal values of input parameters) and measurement results. The frequency deviation of BRB harmonics is minimized by running the simulation at the average slip that is computed from the average measured speed. It can be observed that the amplitude of BRB harmonics significantly varies for four cases. In Case IV, the amplitude deviation is significantly minimized and fairly matched with measurement results. This is reasonable as decreasing the value of the air gap and the B-H curve introduce high magnetic saturation in the machine. Indisputably, BRB harmonics are highly sensitive to the magnetic saturation effect, which significantly reduces the amplitude of BRB harmonics. Moreover, lessening the rotor bar conductivity value shifts the operating point slightly, which also contributes to lowering the amplitude of BRB harmonics.

IV. CONCLUSION

This article proposed a non-intrusive uncertainty propagation scheme to calibrate the input parameters in the 2-D FE model of BRB. The PCE approximation of the FE model provides computational efficiency for estimating the sensitivity analysis indices. The most interesting finding is that the amplitude of BRB harmonics is highly susceptible to the air gap, rotor bar conductivity, and B-H curve of the core materials. The proposed calibration approach lessens the amplitude and frequency deviation of BRB harmonics. The calibrated BRB faults data can be used to build robust ML-based classifiers. This universal approach can be applied to calibrate the input parameters of the FE model for other types of faults, such as eccentricity. In that case, new input parameters may add to the sensitive parameters profile with the existing ones for BRB.

ACKNOWLEDGMENT

This work was supported in part by the Academy of Finland Consortium under Grant 330747.

REFERENCES

[1] B. Asad, T. Vaimann, A. Belahcen, A. Kallaste, A. Rassõlkin, and M. N. Iqbal, "Broken rotor bar fault detection of the grid and inverter-fed induction motor by effective attenuation of the fundamental component," *IET Electr. Power Appl.*, vol. 13, no. 12, pp. 2005–2014, Dec. 2019.

[2] I. Martin-Diaz, D. Morinigo-Sotelo, O. Duque-Perez, and R. J. Romero-Troncoso, "An experimental comparative evaluation of machine learning techniques for motor fault diagnosis under various operating conditions," *IEEE Trans. Ind. Appl.*, vol. 54, no. 3, pp. 2215–2224, May/Jun. 2018.

[3] B. Bessam, A. Menacer, M. Boumehraz, and H. Cherif, "Detection of broken rotor bar faults in induction motor at low load using neural network," *ISA Trans.*, vol. 64, pp. 241–246, Sep. 2016.

[4] J. F. Watson and D. G. Dorrell, "The use of finite element methods to improve techniques for the early detection of faults in 3-phase induction motors," *IEEE Trans. Energy Convers.*, vol. 14, no. 3, pp. 655–660, Sep. 1999.

[5] J. Sprooten and J. C. Maun, "Influence of saturation level on the effect of broken bars in induction motors using fundamental electromagnetic laws and finite element simulations," *IEEE Trans. Energy Convers.*, vol. 24, no. 3, pp. 557–564, Sep. 2009.

[6] P. Offermann, H. Mac, T. T. Nguyen, S. Clénet, H. De Gersem, and K. Hameyer, "Uncertainty quantification and sensitivity analysis in electrical machines with stochastically varying machine parameters," *IEEE Trans. Magn.*, vol. 51, no. 3, pp. 1–4, Mar. 2015.

[7] G. Bramerdorfer, "Tolerance analysis for electric machine design optimization: Classification, modeling and evaluation, and example," *IEEE Trans. Magn.*, vol. 55, no. 8, pp. 1–9, Aug. 2019.

[8] M. Li, M. H. Mohammadi, T. Rahman, and D. Lowther, "Analysis and design of electrical machines with material uncertainties in iron and permanent magnet," *COMPEL-Int. J. Comput. Math. Electr. Electron. Eng.*, vol. 36, no. 5, pp. 1326–1337, Sep. 2017.

[9] J. Martinez, A. Belahcen, and A. Arkkio, "Broken bar indicators for cage induction motors and their relationship with the number of consecutive broken bars," *IET Electr. Power Appl.*, vol. 7, no. 8, pp. 633–642, Sep. 2013.

[10] D. Xiu and G. E. Karniadakis, "The Wiener–Askey polynomial chaos for stochastic differential equations," *SIAM J. Sci. Comput.*, vol. 24, no. 2, pp. 619–644, Jul. 2002.

[11] Y. C. Pati, R. Rezaiifar, and P. S. Krishnaprasad, "Orthogonal matching pursuit: Recursive function approximation with applications to wavelet decomposition," in *Proc. 27th Asilomar Conf. Signals, Syst. Comput.*, 1993, pp. 40–44.

[12] G. Blatman and B. Sudret, "Adaptive sparse polynomial chaos expansion based on least angle regression," *J. Comput. Phys.*, vol. 230, no. 6, pp. 2345–2367, Mar. 2011.

[13] I. M. Sobol, "Sensitivity analysis for non-linear mathematical models," *Math. Modell. Comput. Exp.*, vol. 1, no. 4, pp. 407–414, 1993.

[14] B. Sudret, "Global sensitivity analysis using polynomial chaos expansions," *Rel. Eng. Syst. Saf.*, vol. 93, no. 7, pp. 964–979, Jul. 2008.

[15] S. Marelli and B. Sudret, "UQLab: A framework for uncertainty quantification in MATLAB," in *Proc. 2nd ICVRAM*, 2014, pp. 2554–2563.